Sharma et al. Discover Nano (2026) 21:84
https://doi.org/10.1186/s11671-026-04538-1

Discover Nano

RESEARCH Open Access

Design and optimization of highly sensitive and tunable nanostructure biosensor for heavy metal detection using machine learning

Yogesh Sharma[1*], Trupti Kamani[2], Zaid Ahmed Shamsan[3*] and Shobhit K. Patel[4]

*Correspondence:
Yogesh Sharma
yogesh.sharma2@sharda.ac.in
Zaid Ahmed Shamsan
zashamsan@imamu.edu.sa
[1]Department of Physics and Environmental Sciences, Sharda School of Engineering and Science, Sharda University, Greater Noida, Uttar Pradesh 201310, India
[2]Department of Physics, Marwadi University, Rajkot 360003, India
[3]Department of Electrical Engineering, College of Engineering, Imam Mohammad Ibn Saud Islamic University (IMSIU), 11432 Riyadh, Saudi Arabia
[4]Department of Computer Engineering- AI and Big Data, Marwadi University, Rajkot 360003, India

Abstract

The third biggest concentration of metallic ions is traces of the element copper (Cu^{2+}), which is crucial to all living creatures and plays a key role in several operations. However, deficiency or excessive copper ions may trigger a wide range of disorders, as determined by cellular requirements. To identify these factors, optical SPR-based refractive index sensors have emerged that concentrate on the swift identification of Cu2+ions in the present moment, that has excellent selectivity and sensitivity. Here, this paper intends to design and discuss a Four-Quadrant Circular Grid Refractive Index Biosensor (FQCGRIB) with a machine learning approach for detecting heavy metals like Cu^{2+}. The four-quadrant circular grid refractive index biosensor enhances conventional biosensor performance via improved accuracy, sensitivity, specificity, and detection efficiency. significant sensitivity values of 719.85 nm/RIU, 763.35 nm/RIU, 761.90 nm/RIU, and 734.52 nm/RIU are achieved for $n2cu^{2+}$, $n3cu^{2+}$, $n4cu^{2+}$, and $n5cu^{2+}$, respectively. Simultaneously, a greater detection range of 1175.46, 1175.14, 1176.47, 1189.56, and 1180.59, along with a greater quality factor of 835.35 nm/RIU, 828.85 nm/RIU, 827.72 nm/RIU, 843.21 nm/RIU, and 828.57 nm/RIU, for the $n1cu^{2+}$, $n2cu^{2+}$, $n3cu^{2+}$, $n4cu^{2+}$, and $n5cu^{2+}$, respectively, is obtained. In addition, the minimal achieved detection limit is 0.000932 for $n4cu^{2+}$, and a greater figure of merit is 382.86 for $n4cu^{2+}$. The high predicted value of 0.981494 has been achieved by the machine learning approach for Cu^{2+} ions, and the mean square error value of 0.001987 for Cu^{2+} ions. Along with the results, this sensor has a greater capability with compactness in detecting heavy metal ions.

Keywords Cu^{2+} detection, Surface plasmon resonance, Highly efficient, Medical and environmental application, Biosensor

1 Introduction

Copper ions (Cu^{2+}) have emerged as a transition metallic substance that causes a significant risk to the well-being of humans [1, 2]. These key metal ions play a critical role in many different areas, including the surrounding environment and the health of humans. It serves as a notable function for the human organism as a catalyst component of redox-regulating enzymes, such as a range of metabolic processes [3–5]. In accordance with ordinary circumstances, the human organism doesn't get negatively affected by the Cu^{2+} ions, but excessive or inadequate amounts can trigger some adverse effects. While low levels of the naturally occurring Cu^{2+} ion are adequate for ordinary biological activities, exceeding the usual minimum consumption has detrimental effects on human wellness [6, 7]. Furthermore, the metabolic process of iron is controlled by copper ions, and elevated amounts of this substance or continuous contact with copper can result in a number of disorders. The excessive consumption of Cu^{2+} ions could result in sensations that include vomiting, nausea, anxiety, and gastrointestinal discomfort [7, 8]. The human organism accumulates unbound Cu^{2+} ions as a consequence of continuous exposure, which generate oxygen species that are reactive through redox mechanisms and cause destruction to lipid molecules, genetic material, and protein molecules. These cells could be exposed to toxicity from liberated oxygen molecules [9, 10]. Hemostasis abnormalities can give rise to the occurrence of several infectious diseases in the human body [11, 12]. The EPA (Environmental Protection Agency) limits the concentration of Cu^{2+} ions in the consumption of water to 1.3 ppm [13, 14]. Normal people must have a blood serum copper level ranging from 100–150 μg/dL [15, 16]. Furthermore, agricultural, manufacturing, and residential activities result in Cu2 + ions in the environment as well [17]. Several approaches have been employed to identify metal trace elements. The various techniques of finding the ions of Cu^{2+} include highly sensitive liquid chromatography, induction-coupled plasma atomic emission spectrometry [18, 19], voltammetry with anodic stripping [20], atomic absorption spectrometry [21, 22], and induction-coupled plasma mass spectrometry [23]. Nevertheless, these techniques include pros like speed, precision, and durability, but also cons like costly and complicated steps that need to be addressed [24]. Enhancing sensitivity, as well as easily executed, quick, repeatable, affordable, and accurate methods that can identify Cu^{2+} ions in both environmental and medicinal samples, are urgently needed [25]. Therefore, sensors are tools for analysis that transform environmental changes like physical, chemical, and biological fluctuations into electrical signals [26].

Surface plasmon resonance (SPR) has become a significant kind of optical sensor that relies on the intensity produced by light reflected by a metal-film-covered prism. SPR sensors examine interactions between molecules that took place on the sensor outer layer with the help of surface plasmon (SP) oscillations. SPR sensors offer many positive aspects, including their affordability, no need for labelling, the requirement for a minimal sample size, continuous monitoring, high accuracy and specificity, and the ability to carry out swift measurements [27]. A novel work of square-shaped photonic crystal fiber sensor with 15,800 nm/RIU and 14,300 nm/RIU of wavelength sensitivity, and 11,584 RIU^{-1} and 11,007 RIU^{-1} of amplitude sensitivities, has been presented [28]. The Kagome-inspired surface plasmon resonance-based numerical study of blood detection, with a 10^{-6} RIU of peak sensor resolution sensor has been presented [29]. The heavy metal detection study with various optical methods [30], and refractive index integration with spectroscopy methods detection is achieved [31]. Wenhua Wang et al. present a surface plasmon resonance-based sensor to detect the Cu^{2+} ions. They have used gold and silver film, which has been modified by modified chitosan film, and that has worked as an active layer. After five cycles of extraction using a concentrated EDTA-based solution that contained 0.5 mmol/L, the sensor maintains extraction with capacity ratios exceeding 96%. This SPR-based sensor exhibited a sensitivity of 0.7271 ppm^{-1} within the range of 1 to 5 ppm. The small amount of Cu2 + has a limit of detection (LOD) of 18 ppb [32]. Lijie Zhang et al. propose an optical fiber surface plasmon resonance sensor that is copper-imprinted and employed to identify Cu^{2+} ions. It has used a gold layer to excite the surface plasmon, which enhances the sensitivity of the copper metal ions. Here, this paper demonstrates an ion imprinting methodology that improves overall results in terms of selectivity, sensitivity, etc. The achieved sensitivity is – 10.05 pm/ppm [33]. Mehdi Atapour et al. introduce an optical electrochemical sensor for the measurement of concentrations of Cu^{2+} ions in water. This work developed a biosensor leveraging L-cysteine-gold nanoparticles as well as a transparent-conductive substrate to measure Cu2 + ionic levels in aquatic solutions by electrochemical and optical approaches. The achieved detection limit is 5 nM, and the total linear range is 10–100000 nM [34]. Hongxia Chen et al. developed a quantitative copper ion surface plasmon resonance sensor, which has been used to study the conformational change of Cu^{2+} ions peptides. Therefore, the conformational change that occurs in the Cu^{2+} particular binding peptide allows for the selective and sensitive determination of Cu^{2+}. The detection limit of 0.44 pM, and detection range of 1×10^{-12} M to 1×10^{-6} M have been achieved [35]. Zidan Gong et al. designed a taper-in-taper structure-based fibre sensor for the determination of Cu2 + ions in the drinking water. According to the results of experiments, the designed fiber sensor has a sensitivity of 2741 nm/RIU in a given refractive index (RI) and is approximately 3.7 times more sensitive than ordinary tapered fiber sensors. This sensor is capable of identifying the presence of copper ions with a sensitivity of 78.03 nm/mM at Cu^{2+} concentrations ranging from 0 to 0.1 mM [36].

This paper intends to design and discuss a Four-Quadrant Circular Grid Refractive Index Biosensor (FQCGRIB) for detecting heavy metals like Cu^{2+}, along with the utilization of the machine learning method for predicting the regression and surface plasmon resonance methodology to boost the detection capacity. The working wavelength range of an intended FQCGRIB biosensor is 1580 nm to 1740 nm. Here, this biosensor works on the principle of refractive index.

2 Geometry evolution and numerical analysis

2.1 Biosensor design

The Four-Quadrant Circular Grid Refractive Index Biosensor (FQCGRIB) for detecting heavy metals like Cu^{2+} has been intended in the following biosensor design part. The five different variants of Cu^{2+} by names, n1Cu^{2+}, n2Cu^{2+}, n3Cu^{2+}, n4Cu^{2+}, and n5Cu^{2+}, with refractive index values of 1.33248, 1.34915, 1.35606, 1.36398, and 1.3706, respectively. The FQCGRIB enhances conventional biosensor performance by improving accuracy, sensitivity, specificity, and efficiency of detection. The quadrant-based segmentation in the biosensor design can allow the sensor to perform multi-point sensing, which can increase the accuracy by minimizing external interference. The circular grid structure of the biosensor optimizes light propagation to ensure corresponding interaction among analytes and appropriate refractive index assessments. Moreover, this design additionally enables multiplexing, facilitating the need for the simultaneous identification across multiple substances. The symmetrical configuration contributes to reproducible results, which leads to reliable results throughout several assessments. By assembling these attributes, the biosensor achieves greater sensitivity, reduced detection limits, and selective properties, thus serving as a good choice for modern applications in new research areas.

Here, the substrate material we have chosen is SiO_2 because it gives excellent optical properties, chemical stability, and a smooth surface to give minimal interference and consistent transmittance of signals. The resonator material we have selected is Ag (silver) for its strong plasmonic properties, which can lead to enhanced detection of refractive index. In addition, a selective dimension of the FQCGRIB is an essential part of the sensor while designing it for detection accuracy and efficiency. The selective dimension of the FQCGRIB biosensor of the SiO2-substrate breadth (SSB) value is 200 nm, the SiO2-substrate lengthiness (SSL) value is 3000 nm, and the space between each quadrant (SQ) is 100 nm. The inner circular grid radius 1 (IGR_1) is 800 nm, while the outer circular grid radius 2 (IGR_2) is 1000 nm. The graphical view of the Four-Quadrant Circular Grid Refractive Index Biosensor (FQCGRIB) is observed in Fig. 1. The perspective representation of the FQCGRIB is observed in Fig. 1A, the top-plane representation of the FQCGRIB is observed in Fig. 1B, and the elevation depiction of the FQCGRIB is observed in Fig. 1C.

2.2 Conventional parameters

This sub-section of the conventional parameters proposes a numerical evolution of the Four-Quadrant Circular Grid Refractive Index Biosensor (FQCGRIB) to detect heavy metals like $Cu^{2+.}$ This numerical evolution has some mathematical equations of sensor resolution, sensitivity, signal to noise ratio, quality factor, detection limit, figure of merit, and detection range from Eq. (1) to Eq. (7) which gives the results in terms of functionality of the biosensor [37, 38]. This functionality of the FCGRIB biosensor also relies on the dimensions and the material we have utilized as substrate and resonator.

$$SR = S \times DL \tag{1}$$

$$S = \frac{\Delta\lambda}{\Delta n} \tag{2}$$

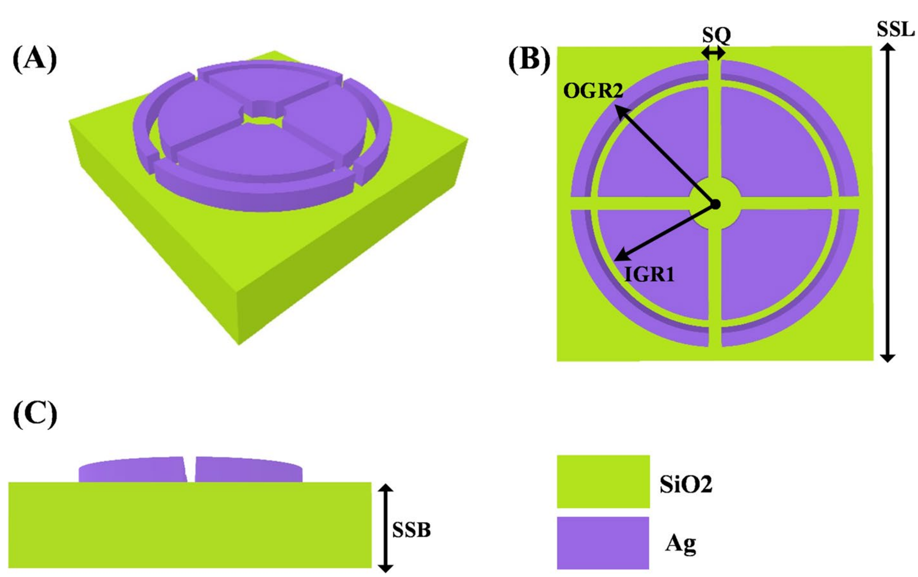

Fig. 1 The graphical view of the intended Four-Quadrant Circular Grid Refractive Index Biosensor (FQCGRIB) **A** Perspective representation of FQCGRIB **B** Top-plan representation of FQCGRIB **C** Elevation depiction of FQCGRIB

$$SNR = \frac{\Delta\lambda}{FWHM} \tag{3}$$

$$Q = \frac{\lambda}{FWHM} \tag{4}$$

$$DL = \left(\frac{\Delta n}{1.5}\right) \times \left(\frac{FWHM}{\Delta\lambda}\right)^{1.25} \tag{5}$$

$$FOM = \frac{S}{FWHM} \tag{6}$$

$$DR = \frac{\lambda}{\sqrt{FWHM}} \tag{7}$$

3 Results and discussions

The Four-Quadrant Circular Grid Refractive Index Biosensor (FQCGRIB) has been tailored with distinctive geometrical and operational properties that optimize its capability to distinguish Cu^{2+} metal ions. This section of results and discussion proposes an optimization of the geometry dimensions in terms of the graphs of the wavelength versus transmittance. This section shows how these geometric dimensions affect the sensor results while changes are made in the dimensions. The working wavelength range of an intended FQCGRIB biosensor is 1580 nm to 1740 nm.

Figure 2 proposes the anatomization of the conventional parameters of the Four-Quadrant Circular Grid Refractive Index Biosensor (FQCGRIB), which refers to the space between each quadrant (SQ) in nm selective dimension. Figure 2A proposes an anatomization of the space between each quadrant, SQ = 50 nm, with an observed shift in the right side, whilst Fig. 2B proposes an anatomization of the space between each quadrant, SQ = 100 nm. Figure 2C proposes an anatomization of the space between each quadrant, SQ = 150 nm, along with an observed shift in the left side. Figure 2D proposes an anatomization of the space between each quadrant, SQ = 200 nm with left side wavelength shift & missing of the $n1cu^{2+}$ peak, and Fig. 2E proposes an anatomization of the space between each quadrant, SQ = 250 nm. In this case, Fig. 2B greatly impacts the conventional parameters of its response, specifically at a dimension of the space between each quadrant, SQ = 100 nm of the FQCGRIB. At this configuration, high sensitivity values of 719.85 nm/RIU, 763.35 nm/RIU, 761.90 nm/RIU, and 734.52 nm/RIU for $n2cu^{2+}$, $n3cu^{2+}$, $n4cu^{2+}$, and $n5cu^{2+}$, respectively, are achieved. Here, $n1cu^{2+}$ is taken as a reference point. A larger detection range of 1175.46, 1175.14, 1176.47, 1189.56, and 1180.59, along with higher quality factors of 835.35 nm/RIU, 828.85 nm/RIU, 827.72 nm/RIU, 843.21 nm/RIU, and 828.57 nm/RIU, are achieved for $n1cu^{2+}$, $n2cu^{2+}$, $n3cu^{2+}$, $n4cu^{2+}$, and $n5cu^{2+}$, respectively. The minimal achieved detection limit is 0.000932 for $n4cu^{2+}$, and a greater figure of merit is 382.86 for $n4cu^{2+}$. Figure 2E shows that one group of metal ions shifts completely to the left and disappears, while another group of metal ions is observed with very high transmittance.

Figure 3 proposes the anatomization of the conventional parameters of the FQCGRIB, which refers to the SiO_2-substrate lengthiness (SSL) in nm selective dimension. Figure 3A proposes an anatomization of the SiO_2-substrate lengthiness, SSL = 3000 nm, whilst Fig. 3B proposes an anatomization of the SiO_2-substrate lengthiness, SSL = 3100 nm,

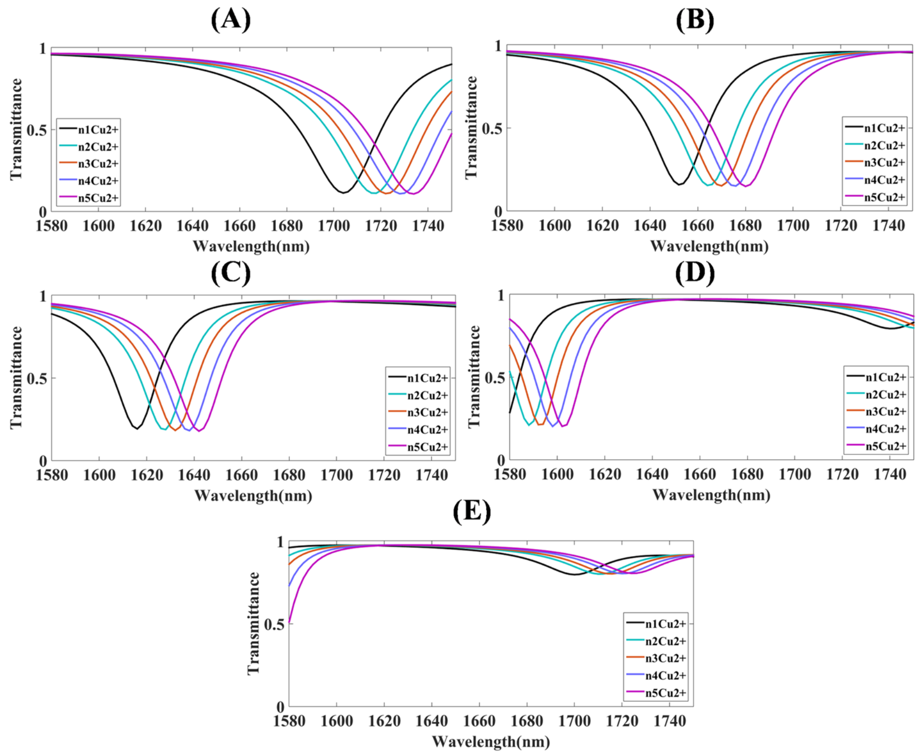

Fig. 2 The anatomization of the conventional parameters of the Four-Quadrant Circular Grid Refractive Index Biosensor (FQCGRIB), which refers to the space between each quadrant (SQ) in nm selective dimension **A** SQ = 50 **B** SQ = 100 **C** SQ = 150 **D** SQ = 200 **E** SQ = 250

along with an additional set of Cu^{2+} ions. Figure 3C proposes an anatomization of the SiO_2-substrate lengthiness, SSL = 3200 nm, and it has higher transmittance than Fig. 3A, which creates a distraction while detecting copper metal ions. Figure 3D proposes an anatomization of the SiO_2-substrate lengthiness, SSL = 3300 nm, and Fig. 3E proposes an anatomization of the SiO_2-substrate lengthiness, SSL = 3400 nm. In this case, Fig. 3A greatly impacts conventional parameters of its response, specifically at a dimension of the SiO_2-substrate lengthiness, SSL = 3000 nm of the FQCGRIB. Larger detection sensitivity values of 719.85 nm/RIU, 763.35 nm/RIU, 761.90 nm/RIU, and 734.52 nm/RIU for $n2cu^{2+}$, $n3cu^{2+}$, $n4cu^{2+}$, and $n5cu^{2+}$, respectively, are achieved. Here, $n1cu^{2+}$ is taken as a reference point. The achieved greater detection range of 1175.46, 1175.14, 1176.47, 1189.56, and 1180.59, as well as greater quality factors of 835.35 nm/RIU, 828.85 nm/RIU, 827.72 nm/RIU, 843.21 nm/RIU, and 828.57 nm/RIU, for $n1cu^{2+}$, $n2cu^{2+}$, $n3cu^{2+}$, $n4cu^{2+}$, and $n5cu^{2+}$, respectively, are accomplished. The minimal achieved detection limit is 0.000932 for $n4cu^{2+}$, and a greater figure of merit is 382.86 for the same ions. Figure 3D, E have three sets of copper ions with very low sensitivity and high transmittance rates.

Figure 4 proposes the anatomization of the conventional parameters of the Four-Quadrant Circular Grid Refractive Index Biosensor (FQCGRIB), which refers to the inner circular grid radius 1 (IGR_1) in nm selective dimension. Figure 4A proposes an anatomization of the inner circular grid radius 1, IGR_1 = 700 nm, with no peaks of any copper ion metal, whilst Fig. 4B proposes an anatomization of the inner circular grid radius 1, IGR_1 = 750 nm, it shows that the first peak is not in the operating range that's why this dimension of the geometry is not suited. Figure 4C proposes an anatomization

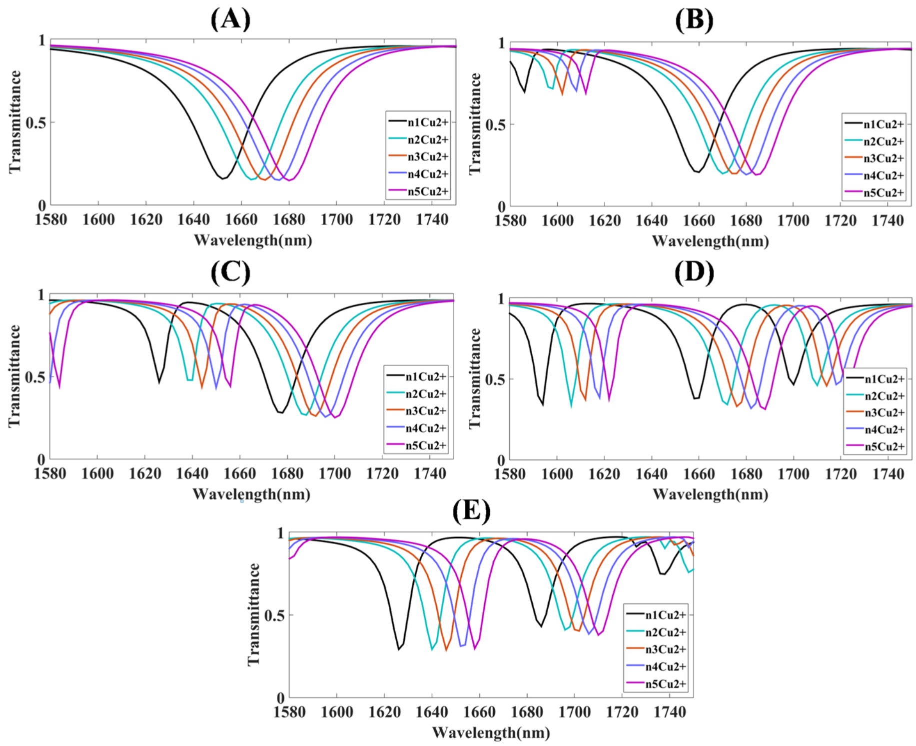

Fig. 3 The anatomization of the conventional parameters of the Four-Quadrant Circular Grid Refractive Index Biosensor (FQCGRIB), which refers to the SiO_2-substrate lengthiness (SSL) in nm selective dimension **A** SSL = 3000 **B** SSL = 3100 **C** SSL = 3200 **D** SSL = 3300 **E** SSL = 3400

of the inner circular grid radius 1, IGR_1 = 800 nm. Figure 4D proposes an anatomization of the inner circular grid radius 1, IGR_1 = 850 nm, and Fig. 4E proposes an anatomization of the inner circular grid radius 1, IGR_1 = 900 nm. In this case, Fig. 4C greatly impacts the conventional parameters of its response, specifically at a dimension of the inner circular grid radius 1, IGR_1 = 800 nm of the FQCGRIB. High sensitivity of 719.85 nm/RIU, 763.35 nm/RIU, 761.90 nm/RIU, and 734.52 nm/RIU is accomplished for n2cu^{2+}, n3cu^{2+}, n4cu^{2+}, and n5cu^{2+}, respectively. Here, n1cu^{2+} is taken as a reference point. Larger detection range of 1175.46, 1175.14, 1176.47, 1189.56, and 1180.59, and a greater quality factor of 835.35 nm/RIU, 828.85 nm/RIU, 827.72 nm/RIU, 843.21 nm/RIU, and 828.57 nm/RIU, is achieved for the n1cu^{2+}, n2cu^{2+}, n3cu^{2+}, n4cu^{2+}, and n5cu^{2+}, respectively. The minimal achieved detection limit is 0.000932 for n4cu^{2+}, and a greater figure of merit is 382.86 for n4cu^{2+}. Additionally, Fig. 4D shows that it has two sets of Cu^{2+} ions, in which the left side set is high transmittance, and the right side set of peaks is not in the operating range. Figure 4E also illustrates that it has two sets of peaks, but the left side set of peaks is not in the operating range, and the right side set has high transmittance.

Figure 5 proposes the anatomization of the conventional parameters of the Four-Quadrant Circular Grid Refractive Index Biosensor (FQCGRIB), which refers to the SiO_2-substrate breadth (SSB) in nm selective dimension. Figure 5A presents an analysis of the SiO_2-substrate breadth, SSB = 110 nm, along with some distraction by unnecessary peaks, whilst Fig. 5B presents an analysis of the SiO_2-substrate breadth, SSB = 140 nm, with a higher transmittance of around 25% to 30% than that of Fig. 5D. Figure 5C proposes an anatomization of the SiO_2-substrate breadth, SSB = 170 nm. Figure 5D proposes an anatomization of the SiO_2-substrate breadth, SSB = 200 nm, and Fig. 5E proposes

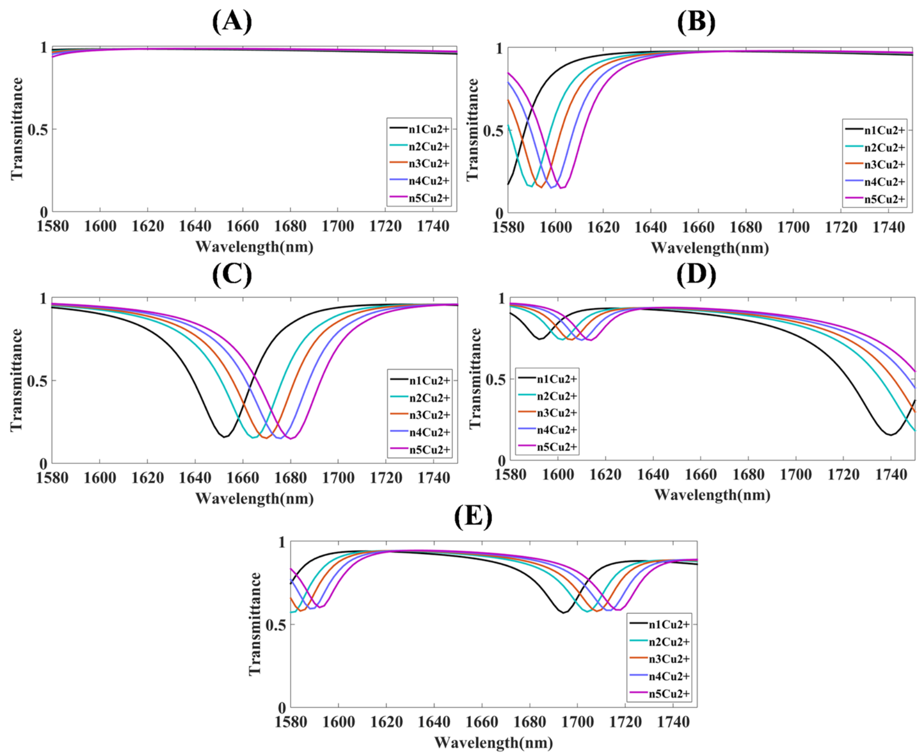

Fig. 4 The anatomization of the conventional parameters of the Four-Quadrant Circular Grid Refractive Index Biosensor (FQCGRIB), which refers to the inner circular grid radius 1 (IGR_1) in nm selective dimension **A** $IGR_1 = 700$ **B** $IGR_1 = 750$ **C** $IGR_1 = 800$ **D** $IGR_1 = 850$ **E** $IGR_1 = 900$

an anatomization of the SiO_2-substrate breadth, SSB = 230 nm. In this case, Fig. 5D greatly impacts the conventional parameters of its response, specifically at a dimension of the SiO_2-substrate breadth, SSB = 200 nm of FQCGRIB. Higher sensitivity values of 719.85 nm/RIU, 763.35 nm/RIU, 761.90 nm/RIU, and 734.52 nm/RIU for $n2cu^{2+}$, $n3cu^{2+}$, $n4cu^{2+}$, and $n5cu^{2+}$, respectively, are achieved. Here, $n1cu^{2+}$ is taken as a reference point. Larger detection range of 1175.46, 1175.14, 1176.47, 1189.56, and 1180.59, along with a greater quality factor of 835.35 nm/RIU, 828.85 nm/RIU, 827.72 nm/RIU, 843.21 nm/RIU, and 828.57 nm/RIU, is acquired for $n1cu^{2+}$, $n2cu^{2+}$, $n3cu^{2+}$, $n4cu^{2+}$, and $n5cu^{2+}$, respectively. The minimal achieved detection limit is 0.000932 for $n4cu^{2+}$, and a greater figure of merit is 382.86 for $n4cu^{2+}$. Here, Fig. 5C–E look similar, but there are some differences in sensitivity, quality factor, and detection limits.

Figure 6 proposes the anatomization of the conventional parameters of the Four-Quadrant Circular Grid Refractive Index Biosensor (FQCGRIB), which refers to the outer circular grid radius 2 (OGR_2) in nm selective dimension. Figure 6A proposes an anatomization of the outer circular grid radius 2, $OGR_2 = 800$ nm, with 40% of high transmittance rates, whilst Fig. 6B proposes an anatomization of the outer circular grid radius 2, $OGR_2 = 900$ nm, with two sets of copper metal ions, but none of this has proper alinement with operating range. Figure 6C proposes an anatomization of the outer circular grid radius 2, $OGR_2 = 1000$ nm. Figure 6D proposes an anatomization of the outer circular grid radius 2, $OGR_2 = 1100$ nm, and Fig. 6E proposes an anatomization of the outer circular grid radius 2, $OGR_2 = 1200$ nm. In this case, Fig. 6C greatly impacts conventional parameters of its response, specifically at a dimension of the outer circular grid radius 2, $OGR_2 = 1000$ nm of the FQCGRIB. It has been seen that larger sensitivity of

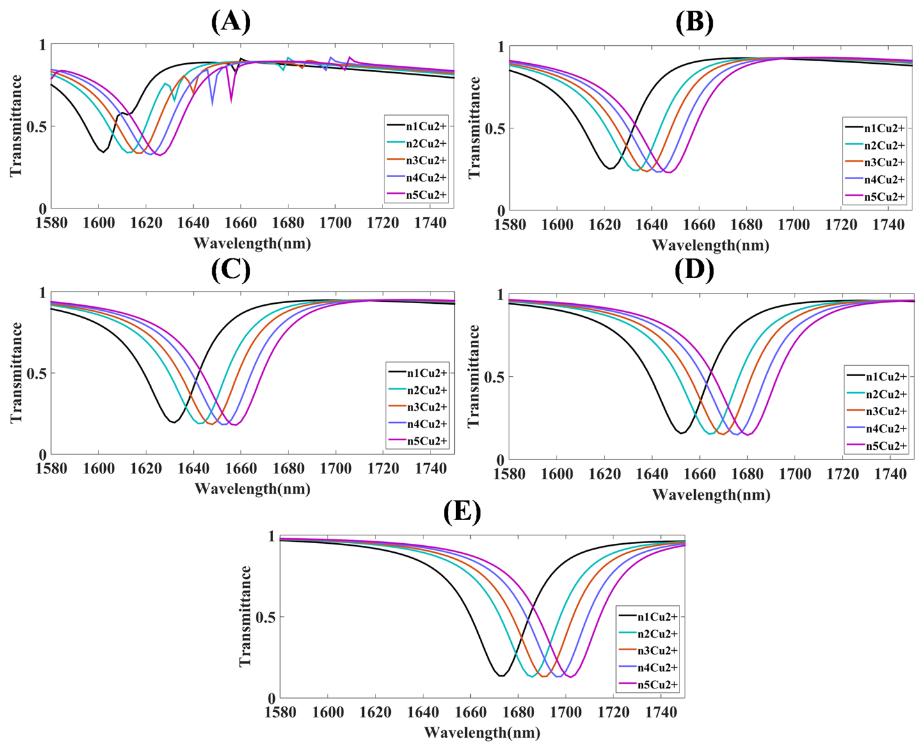

Fig. 5 The anatomization of the conventional parameters of the Four-Quadrant Circular Grid Refractive Index Biosensor (FQCGRIB), which refers to the SiO_2-substrate breadth (SSB) in nm selective dimension **A** SSB = 110 **B** SSB = 140 **C** SSB = 170 **D** SSB = 200 **E** SSB = 230

719.85 nm/RIU, 763.35 nm/RIU, 761.90 nm/RIU, and 734.52 nm/RIU has been achieved for n2cu^{2+}, n3cu^{2+}, n4cu^{2+}, and n5cu^{2+}, respectively. Here, n1cu^{2+} is taken as a reference point. Also, the achieved greater detection range is 1175.46, 1175.14, 1176.47, 1189.56, and 1180.59, and the corresponding greater quality factor is 835.35 nm/RIU, 828.85 nm/RIU, 827.72 nm/RIU, 843.21 nm/RIU, and 828.57 nm/RIU, for the n1cu^{2+}, n2cu^{2+}, n3cu^{2+}, n4cu^{2+}, and n5cu^{2+}, in the same order. Similarly, the minimal achieved detection limit is 0.000932 for n4cu^{2+}, and the greater figure of merit is 382.86 for n4cu^{2+}. Figure 6D, E showed somewhat less impact on the conventional parameters of the intended biosensor than that in Fig. 6C. The proposed Table 1 introduces the response of the Conventional parameters of the FQCGRIB to recognize heavy metal ions.

4 Machine learning approach

A machine learning (ML) model was used in this work to enhance the predictive power of the suggested FQCGRIB sensor by relating the pattern of the predicted surface plasmon resonance (SPR) and the resulting changes in refractive indices caused by Cu^{2+} ions. The simulated spectra yielded input values in the form of resonance wavelength shifts, full width at half maximum, and quality factor values, which were used as predictors in a linear regression model. The data set was obtained through a great deal of parametric simulation in a variety of values of the refractive index to obtain diversity and strength of the training data. To prove the stability of the model, the data were split into training and testing sets, and k fold cross validation was used to assess the generalization performance. The machine learning approach offered better prediction to noise or multifaceted parameter interactions compared to the traditional methods of analysis or

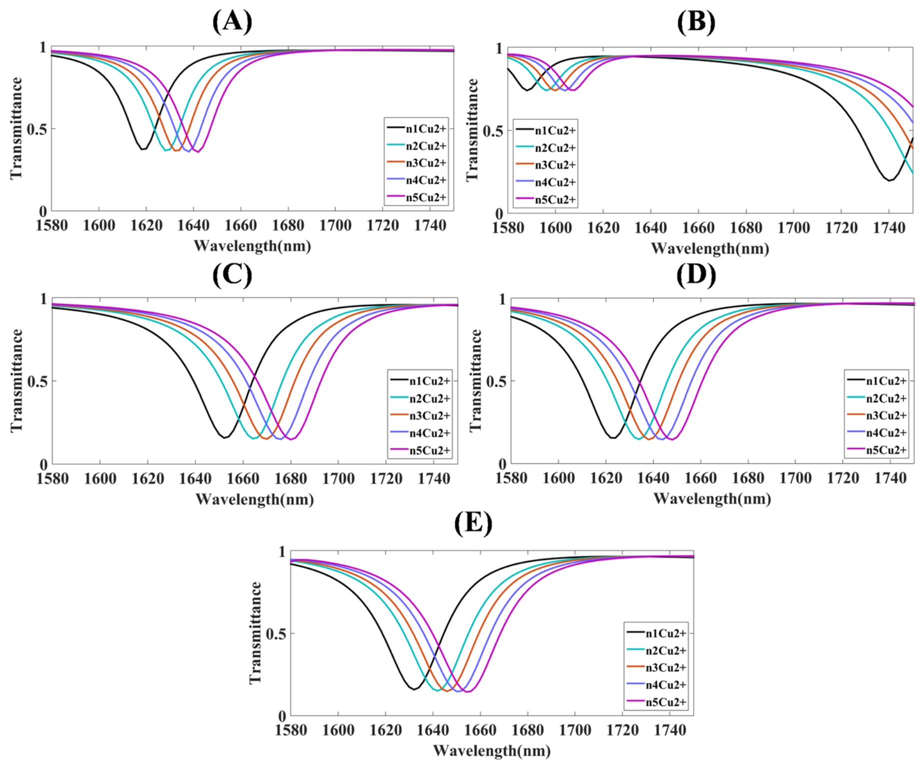

Fig. 6 The anatomization of the conventional parameters of the Four-Quadrant Circular Grid Refractive Index Biosensor (FQCGRIB), which refers to the outer circular grid radius 2 (OGR_2) in nm selective dimension **A** $OGR_2 = 800$ **B** $OGR_2 = 900$ **C** $OGR_2 = 1000$ **D** $OGR_2 = 1100$ **E** $OGR_2 = 1200$

Table 1 Conventional parameters of the Four-Quadrant Circular Grid Refractive Index Biosensor (FQCGRIB) to recognize heavy metal ions

Heavy metal ions	Refractive index (n)	Difference in the refractive index (Δn)	Peak Wavelength (nm)	Sensitivity (nm/RIU)	Detection limit (DL)	Detection Range (DR)	Quality factor (QF)	Figure of merit (FOM)	Sensor Resolution (SR)	Signal Noise Ratio (SNR)
n1Cu^{2+} (Reference)	1.33248	Ref	1654	Ref	Ref	1175.46	835.35	363.56	Ref	6.0606
n2Cu^{2+}	1.34915	0.01667	1666	719.85	0.001188	1175.14	828.85	358.13	0.8551	5.9701
n3Cu^{2+}	1.35606	0.02358	1672	763.35	0.001020	1176.47	827.72	377.89	0.7786	8.9108
n4Cu^{2+}	1.36398	0.0315	1678	761.90	0.000932	1189.56	843.21	382.86	0.7100	12.0603
n5Cu^{2+}	1.3706	0.03812	1682	734.52	0.000944	1180.59	828.57	361.83	0.6933	12.1739

numerical techniques that depend on a priori assumptions and may also be constrained by their ability to estimate error levels. The application of a linear regression model therefore also explains the incorporation of machine learning as it provides a scalable, interpretive, and flexible framework that improves the quantitative relationship between sensor response and the analyte concentration as well as underscores its superiority to more traditional approaches in the context of accuracy and strength.

This MLapproach is discussed in the following section of the intended (FQCGRIB. The machine learning approach gives an idea of the predicted value. The graph of machine learning prediction is proposed in Fig. 7, with an actual value versus predicted value for

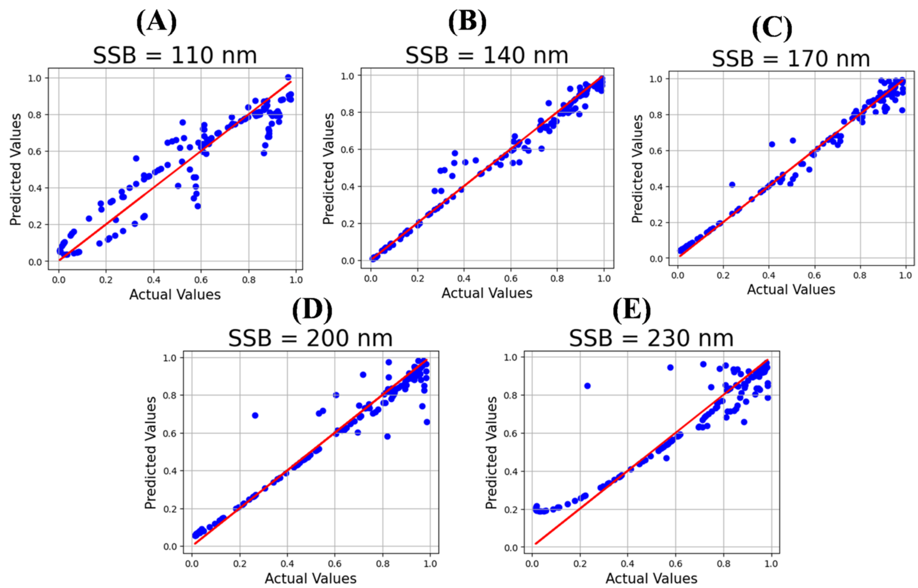

Fig. 7 Machine learning approach applied on the SiO_2-substrate breadth (SSB) geometry parameter (nm) of the Four-Quadrant Circular Grid Refractive Index Biosensor (FQCGRIB) along with the predicted regression value versus actual value **A** SSB = 110 **B** SSB = 140 **C** SSB = 170 **D** SSB = 200 **E** SSB = 230

Table 2 Comparison Table of Four-Quadrant Circular Grid Refractive Index Biosensor (FQCGRIB) conventional parameters to that previously published research

Previously published research references with FQCGRIB	Detection limit (DL)	Sensitivity (nm/RIU)	Figure of merit (FOM)	Quality factor (QF)
[39]	–	570	4	–
[40]	0.0015	714.28	301.38	660.75
[41]	1.013	300	1.796	4.73
[42]	–	166	–	3702
[43]	0.16	378	–	–
[44]	–	800	–	–
[45]	0.002	–	–	262
Intended work	0.000932	763.35	382.86	843.21

the geometry parameter SiO_2-substrate breadth (SSB). The geometrical dimensions of the SSB have ranged from 110 to 230 nm. The prediction has been plotted for the particular dimension values like SSB = 110 nm (Fig. 7A), SSB = 140 nm (Fig. 7B), SSB = 170 nm (Fig. 7C), SSB = 200 nm (Fig. 7D), and SSB = 230 nm (Fig. 7E). The R^2 analysis values of the ML are 0.889954, 0.977654, 0.981494, 0.946982, and 0.885215, with a mean square error value of 0.010506, 0.002466, 0.001987, 0.005490, 0.010598, respectively. Here, the high predicted value of 0.981494 has been achieved. The proposed machine learning approach can help to identify minor changes in the refractive index values caused by heavy metal ions, which makes the detection process more reliable by leveraging pattern analysis methods. The proposed Table 2 shows a comparison of the FQCGRIB conventional parameters with the previously published research parameters.

5 Conclusion

Optical sensors frequently find application across environmental usage, pharmacological and biological studies, and health services to identify various biomolecules for the detection of health issues. In this study of research work, we have designed a novel Four-Quadrant Circular Grid Refractive Index Biosensor (FQCGRIB) to identify Cu^{2+} metal ions. This work includes the study of five types of copper ions detection by the names, $n1Cu^{2+}$, $n2Cu^{2+}$, $n3Cu^{2+}$, $n4Cu^{2+}$, and $n5Cu^{2+}$, with refractive index values of 1.33248, 1.34915, 1.35606, 1.36398, and 1.3706, respectively. The section of results and discussion proposes an optimization of the geometry dimensions in terms of the graphs of the wavelength versus transmittance. It is found that the achieved greater sensitivity is 719.85 nm/RIU, 763.35 nm/RIU, 761.90 nm/RIU, and 734.52 nm/RIU for $n2cu^{2+}$, $n3cu^{2+}$, $n4cu^{2+}$, and $n5cu^{2+}$, respectively. In addition, the achieved greater detection range is 1175.46, 1175.14, 1176.47, 1189.56, and 1180.59, and the corresponding greater quality factor is 835.35 nm/RIU, 828.85 nm/RIU, 827.72 nm/RIU, 843.21 nm/RIU, and 828.57 nm/RIU, for $n1cu^{2+}$, $n2cu^{2+}$, $n3cu^{2+}$, $n4cu^{2+}$, and $n5cu^{2+}$, respectively. Further, the minimal achieved detection limit is 0.000932 for $n4cu^{2+}$, and the greater figure of merit is 382.86 for $n4cu^{2+}$. Moreover, the high predicted value of 0.981494 has been achieved by the machine learning approach for Cu^{2+} ions, and the mean square error value of 0.001987 for Cu^{2+} ions. Although the suggested FQCGRIB sensor has a high sensitivity and tunability in the detection of Cu2 +, some limitations in the form of complexity of fabricating a sensor, tolerance control, and possible interference of matrices still exist. The future perspective is, in general, developing scalable nanofabrication techniques, combining powerful surface functionalization plans, and expanding the design to multiplexed sensing of various heavy metals to a wider environmental and biomedical purpose.

Acknowledgements
Not applicable.

Author contributions
Methodology, Y.S. and T.K.,; software, Y.S., T.K, and Z.A.S.; investigation, Y.S., T.K., and S.K.P.; Formal Analysis, All Authors.; writing—original draft preparation, All Authors.; writing—review and editing, All Authors.; All authors have read and agreed to the published version of the manuscript.

Funding
Open access funding provided by Sharda University. This work was supported and funded by the Deanship of Scientific Research at Imam Mohammad Ibn Saud Islamic University (IMSIU) (grant number IMSIU-DDRSP2604).

Data availability
The data supporting the findings in this work are available from the corresponding author with reasonable request.

Declarations

Ethics approval and consent to participate
Not applicable.

Consent for publication
Not applicable.

Competing interests
The authors declare no competing interests.

Received: 9 December 2025 / Accepted: 18 March 2026
Published online: 26 March 2026

References

1. Karakuş E. A rhodamine based fluorescent chemodosimeter for the selective and sensitive detection of copper (II) ions in aqueous media and living cells. J Mol Struct. 2021. https://doi.org/10.1016/j.molstruc.2020.129037.

2. Yu J, et al. Fabrication of the Ni-based composite wires for electrochemical detection of copper(Ⅱ) ions. Anal Chim Acta. 2021;1143:45–52. https://doi.org/10.1016/j.aca.2020.11.028.
3. Chen X, et al. New fluorescent and colorimetric chemosensors bearing rhodamine and binaphthyl groups for the detection of Cu2+. Sens Actuators B Chem. 2009. https://doi.org/10.1016/j.snb.2009.02.010.
4. Hu L, et al. A high-performance fluorescent and ratiometric colorimetric detection of Cu2+ in practice. Anal Methods. 2023. https://doi.org/10.1039/d3ay01082a.
5. Kumar V, Kalita J, Bora HK, Misra UK. Relationship of antioxidant and oxidative stress markers in different organs following copper toxicity in a rat model. Toxicol Appl Pharmacol. 2016. https://doi.org/10.1016/j.taap.2016.01.007.
6. Kaykhaii M, Khajeh M, Hashemi SH. Magnetic molecularly imprinted polymer nanoparticles for selective extraction of copper from aqueous solutions prior to its flame atomic absorption determination. J Anal Chem. 2015. https://doi.org/10.1134/S1061934815110106.
7. Duan JX, Li X, Zhang CC. The synthesis and adsorption performance of polyamine Cu2+ imprinted polymer for selective removal of Cu2+. Polym Bull. 2017. https://doi.org/10.1007/s00289-017-1905-6.
8. Khan M, et al. Synthesis of nanostructured novel ion-imprinted polymer for selective removal of Cu2+ and Sr2+ ions from reverse osmosis concentrated brine. Environ Res. 2023. https://doi.org/10.1016/j.envres.2023.116024.
9. Sakunkaewkasem S, et al. Dual-analyte fluorescent sensor based on [5]Helicene derivative with super large Stokes Shift for the selective determinations of Cu2+ or Zn2+ in buffer solutions and its application in a living cell. ACS Sens. 2018. https://doi.org/10.1021/acssensors.8b00158.
10. Abu-Dalo MA, Salam AA, Nassory NS. Ion imprinted polymer based electrochemical sensor for environmental monitoring of copper(II). Int J Electrochem Sci. 2015. https://doi.org/10.1016/s1452-3981(23)06761-5.
11. Tarnowska M, Krawczyk T. Click chemistry as a tool in biosensing systems for sensitive copper detection. Biosens Bioelectron. 2020. https://doi.org/10.1016/j.bios.2020.112614.
12. Nadimetla DN, Bhosale SV. Tetraphenylethylene AIEgen bearing thiophenylbipyridine receptor for selective detection of copper(ii) ion. New J Chem. 2021. https://doi.org/10.1039/d1nj01001h.
13. Lu Y, et al. Fabric/multi-walled carbon nanotube sensor for portable on-site copper detection in water. Adv Compos Hybrid Mater. 2019. https://doi.org/10.1007/s42114-019-00122-7.
14. Odetola L, Sills S, Morrison S. A pilot study on the feasibility of testing residential tap water in North Carolina: implications for environmental justice and health. J Expo Sci Environ Epidemiol. 2021. https://doi.org/10.1038/s41370-021-00352-2.
15. Jung HS, et al. Coumarin-derived cu2+-selective fluorescence sensor: synthesis, mechanisms, and applications in living cells. J Am Chem Soc. 2009. https://doi.org/10.1021/ja808611d.
16. Potentiometric sensors selective for Cu(II) determination in real water samples and biological fluids based on graphene and MWCNTs modified graphite electrodes. Indian J Chem Sect A 2020. https://doi.org/10.56042/ijca.v59i2.26885.
17. Kirk KA, Andreescu S. Easy-to-use sensors for field monitoring of Copper contamination in water and pesticide-sprayed plants. Anal Chem. 2019. https://doi.org/10.1021/acs.analchem.9b03385.
18. Kong T, et al. Synthesis and identification of artificial antigens for cadmium and copper. Food Chem. 2010. https://doi.org/10.1016/j.foodchem.2010.05.087.
19. Awual MR, Hasan MM, Rahman MM, Asiri AM. Novel composite material for selective copper(II) detection and removal from aqueous media. J Mol Liq. 2019. https://doi.org/10.1016/j.molliq.2019.03.141.
20. Biscaglia F, et al. A comparison between different machine learning approaches combined with anodic stripping voltammetry for Copper ions and pH detection in cell culture media. Chemosensors. 2023. https://doi.org/10.3390/chemosensors11010061.
21. Kılınç Y, Özdoğan N. Remediation of wastewater for Nickel using Copper nanoflowers with detection by flame atomic absorption spectrometry (FAAS). Anal Lett. 2024. https://doi.org/10.1080/00032719.2023.2232482.
22. Acar O, Sankazan Dokumaci R, Yalcinkaya O. Determinations of cadmium, tin, copper, iron, and zinc in food samples by electrothermal and flame atomic absorption spectrometries. Gazi Univ J Sci 2023. https://doi.org/10.35378/gujs.956819
23. Zhao Z, Chen H, Zhang H, Ma L, Wang Z. Polyacrylamide-phytic acid-polydopamine conducting porous hydrogel for rapid detection and removal of copper (II) ions. Biosens Bioelectron. 2017. https://doi.org/10.1016/j.bios.2016.12.047.
24. Liu W, Liu Y, Yuan Z, Lu C. Recent advances in the detection and removal of heavy metal ions using functionalized layered double hydroxides: a review. Ind Chem Mater. 2023. https://doi.org/10.1039/d2im00024e.
25. Chen L, et al. A facile colorimetric method for ultra-rapid and sensitive detection of copper ions in water. J Inorg Organomet Polym Mater. 2022. https://doi.org/10.1007/s10904-022-02255-7.
26. Vigneshvar S, Sudhakumari CC, Senthilkumaran B, Prakash H. Recent advances in biosensor technology for potential applications—an overview. Front Bioeng Biotechnol. 2016. https://doi.org/10.3389/fbioe.2016.00011.
27. Verma R, Gupta BD. Detection of heavy metal ions in contaminated water by surface plasmon resonance based optical fibre sensor using conducting polymer and chitosan. Food Chem. 2015. https://doi.org/10.1016/j.foodchem.2014.06.045.
28. Ramola A, Shakya AK, Bergman A. Finite element method-based modeling of a novel square photonic crystal fiber surface plasmon resonance sensor with a Au–ToO_2 interface and the relevance of artificial intelligence techniques in sensor optimization. Photonics. 2025;12(6):565. https://doi.org/10.3390/photonics12060565.
29. Ramola A, Shakya AK, Droby A, Bergman A. Numerical study of a novel kagome-inspired photonic crystal fiber-based surface plasmon resonance biosensor for detection of blood components and analytical targets. Biosensors. 2025;15(8):539. https://doi.org/10.3390/bios15080539.
30. Shakya AK, Singh S. State of the art in fiber optics sensors for heavy metals detection. Opt Laser Technol. 2022;153:108246. https://doi.org/10.1016/j.optlastec.2022.108246.
31. Ramola A, Shakya AK, Vidyarthi A, Singh S, Talker E, Bergman A. Next-generation photonic-crystal-fiber-based plasmonic sensor for heavy metal detection via spectroscopy and refractive index integration. In: 29th International conference on optical fiber sensors, M. Lopez-Amo Sainz, J. L. Santos, and T. Sun, Eds., SPIE, May 2025, p. 489. https://doi.org/10.1117/12.3062891.
32. Wang W, et al. Reusable surface plasmon resonance sensor for rapid detection of Cu2+ based on modified-chitosan thin film as an active layer. Sens Actuators A Phys. 2019;286:59–67. https://doi.org/10.1016/j.sna.2018.12.025.
33. Zhang L, Yang W, Zhang C, Pan R, Chen Q, Zhang L. Cu 2+-imprinted optical fiber SPR sensor for intelligent recognition. Opt Express. 2022;30(25):45525. https://doi.org/10.1364/OE.476698.

34. Atapour M, Amoabediny G, Ahmadzadeh-Raji M. Integrated optical and electrochemical detection of Cu2+ ions in water using a sandwich amino acid-gold nanoparticle-based nano-biosensor consisting of a transparent-conductive platform. RSC Adv. 2019. https://doi.org/10.1039/c8ra09659g.
35. Chen H, et al. Sensitive detection of copper(II) ions based on the conformational change of peptides by surface plasmon resonance spectroscopy. Anal Methods. 2015. https://doi.org/10.1039/c5ay02047f.
36. Gong Z, et al. A taper-in-taper structured interferometric optical fiber sensor for Cu2+ ion detection. Sensors. 2022. https://doi.org/10.3390/s22072709.
37. Kamani T, Patel SK, Ben Khalifa S, Pathak P, Chebaane S, Kouki M. Design and optimization of surface plasmon resonance-based non-invasive refractive index biosensor using Ag-SiO2 materials for alcoholic beverages compound detection. Plasmonics. 2025. https://doi.org/10.1007/s11468-025-02914-8.
38. Ali YAA, Kamani T, Patel SK, Saidani T, Almawgani AHM, Alabsi BA. Design and analysis of surface plasmon resonance-based refractive index biosensor for detection of Colorectal Cancer with Machine Learning approach. Plasmonics. 2025. https://doi.org/10.1007/s11468-024-02720-8.
39. Khodaie A, Heidarzadeh H. Design and analysis of a multi-modal refractive index plasmonic biosensor based on split ring resonator for detection of the various cancer cells. Opt Quantum Electron. 2024;56(9):1439. https://doi.org/10.1007/s11082-024-07381-9.
40. Kamani T, Patel SK, A NN, Ghodhbani R, U AK, Armghan A. Design and optimization of surface plasmon resonance refractive index biosensor for early determination of blood cancer and adrenal cancer. Plasmonics. 2025. https://doi.org/10.1007/s11468-025-02868-x.
41. Wekalao J, et al. Graphene-based THz surface plasmon resonance biosensor for hemoglobin detection applicable in Forensic Science. Plasmonics. 2023. https://doi.org/10.1007/s11468-023-02146-8.
42. Krishnamoorthi B, Caroline BE, Michael M, Thirumaran S. A novel rhombic shaped photonic crystal bio-sensor for identifying disorders in the blood samples. Opt Quantum Electron. 2023;55(4):312. https://doi.org/10.1007/s11082-023-04584-4.
43. Saeed AA, Sánchez JLA, O'Sullivan CK, Abbas MN. DNA biosensors based on gold nanoparticles-modified graphene oxide for the detection of breast cancer biomarkers for early diagnosis. Bioelectrochemistry. 2017. https://doi.org/10.1016/j.bioelechem.2017.07.002.
44. Gupta R, et al. GST and MXene-based highly sensitive refractive index sensor with Gold gratings resonator operating for infrared region. Plasmonics. 2024. https://doi.org/10.1007/s11468-024-02517-9.
45. Arunkumar R, Suaganya T, Robinson S. Design and analysis of 2D photonic crystal based biosensor to detect different blood components. Photonic Sensors. 2019;9(1):69–77. https://doi.org/10.1007/s13320-018-0479-8.